DOI: 10.1002/cphc.200800369

Experimental and Theoretical Study of Helium Broadening and Shift of HCO^+ Rotational Lines

Giovanni Buffa,[b] Luca Dore,[c] Francesca Tinti,[c] and Markus Meuwly*[a]

An experimental and theoretical study of pressure broadening and pressure shift of HCO^+ rotational lines perturbed by collisions with He is presented. Results are reported from measurements at 88 K for the lines $j=4\leftarrow3$, $5\leftarrow4$ and $6\leftarrow5$ with frequencies ranging from 0.35 to 0.54 THz. Using a new CCSD(T)/aug-cc-pVQZ potential energy surface for the He–HCO^+ interaction, the collisional line shape parameters are studied from fully quantum and semiclassical calculations. Results from the quantum treatment are in satisfactory agreement with experiments whereas the semiclassical approach can lead to appreciable differences. A study of the dependence of line width Γ and shift s as a function of the translational energy shows the presence of quantum oscillations. Calculations on a previous Hartree–Fock-based potential energy surface lead to quite similar results for the collisional line shape parameters. Using a simplified version of the potential morphing method it is found that the line width Γ is particularly sensitive to the long-range part of the potential energy surface. This also explains the success of the first line-broadening calculations which date back to the 1950s.

1. Introduction

Collisional and radiative excitation are two important mechanisms which determine the existence and shape of spectral lines in the interstellar medium. Therefore a knowledge of collisional rates and of transition moments are needed in order to interpret interstellar spectra in terms of local physical conditions.[1–3] Transition moments are related to the electric dipole moment and are known sufficiently accurately. Collisional rates, on the other hand, are difficult to derive both from experiment and computation. An experimental estimate for collisional rates relies on measurements of collision-induced spectral pressure broadening,[4,5] and a theoretical derivation is based on quantum mechanical scattering calculations. The present work uses both approaches to study He atoms colliding with HCO^+, which is probably the most abundant molecular ion in dense cores of interstellar molecular clouds.[6] While in practice, due to the larger abundance of molecular hydrogen, collisions with *para* H_2 ($j=0$) are more likely in molecular clouds compared to collisions with He atoms, collisional excitation coefficients with H_2 as collision partner can be derived from those with He by applying a scaling factor, as shown by Monteiro.[7]

To the best of our knowledge, no measurements for He colliding with HCO^+ have been presented in the literature so far. Regarding calculations, the only available study[8] is based on a HF/6-311G potential energy surface[9] which, as we show herein, is not accurate. On the other hand, the effect of collisions with Ar atoms on the shape of the HCO^+ rotational lines was widely studied both experimentally and theoretically.[10–13] Recently we presented a study[13] showing good agreement between measurements and quantum calculations based on an accurate Ar–HCO^+ potential energy surface (PES).

Herein, the broadening and shift coefficients for collisions with He at 88 K are measured for the rotational lines $j=4\leftarrow3$, $5\leftarrow4$ and $6\leftarrow5$ of the ion. A new and accurate PES for the He–HCO^+ interaction is obtained and used for quantum and semiclassical calculation of the collisional line shape parameters. Good agreement between experiment and theory is found. The dependence of calculated cross sections on the translational energy is discussed showing that calculations performed at the mean thermal energy are not accurate for this system and that an integration over the thermal energy distribution is needed. Moreover, the presence of quantum oscillations in the energy dependence is found for both the real and imaginary parts of the cross section. Such resonances decay when the translational energy is increased and tend to disappear when it exceeds the depth of the potential well. Finally, to understand better to which parts of the PES collisional line shape parameters are sensitive, potential morphing[14,15] is applied. This procedure shows—not surprisingly—that at low collision energies the calculated observables are mainly sensitive to the long-range part, which is dominated by charge–induced-dipole and dipole–induced-dipole interactions.

Herein, the experimental and computational methods are presented first, followed by a comparison of the measured line widths and the shifts with results from quantum and semiclassical calculations. Next, the dependence of pressure broadening

[a] *Prof. M. Meuwly*
Department of Chemistry
Klingelbergstr. 80, 4056 Basel (Switzerland)
Fax: (+41) 61 267 38 55
E-mail: m.meuwly@unibas.ch

[b] *Dr. G. Buffa*
IPCF-CNR, Largo Pontecorvo 3, 56127 Pisa (Italy)

[c] *Prof. L. Dore, Dr. F. Tinti*
Dipartimento di Chimica "G. Ciamician"
Università di Bologna, Via Selmi 2, 40126 Bologna (Italy)

and shift on the PES is studied by comparing the results obtained from the current CCSD(T)/aug-cc-pVQZ PES and that of ref. [9]. To gain better insight into the sensitivity of the scattering calculations on the shape of the PES in view of the experimental results, morphing transformations of the new PES are carried out and the shifts and widths are recalculated.[14,15]

2. Experimental and Computational Methods

2.1. Experimental Details and Data Analysis

The $j=4\leftarrow3$, $5\leftarrow4$ and $6\leftarrow5$ rotational lines of HCO^+ were observed with a frequency-modulated millimeter-wave spectrometer[16] equipped with a negative glow discharge cell made of a Pyrex tube, 3.25 m long and 5 cm in diameter, with two cylindrical hollow electrodes 25 cm in length at either end. The radiation source was a frequency multiplier, consisting of a doubler in cascade with a multiplier (RPG—Radiometer Physics GmbH), which was driven by a Gunn oscillator working in the region 81–115 GHz (J. E. Carlstrom Co). Two phase-lock loops allow the stabilization of the Gunn oscillator with respect to a frequency synthesizer, which is driven by a 5 MHz rubidium frequency standard. The frequency modulation of the radiation is obtained by sine-wave modulating the reference signal of the wide-band Gunn-synchronizer at 1.666 kHz with low distortion (total harmonic distortion less than 0.01 %). The signal, detected by a liquid-helium-cooled InSb hot electron bolometer (QMC Instr. Ltd. type QFI/2), is demodulated at 2-*f* by a lock-in amplifier.

HCO^+ was produced in a DC discharge by flowing a 1:1 mixture of CO and H_2 at constant pressure with addition of He buffer gas. The discharge in He could not be switched on in the fast flow provided by the diffusion pump employed in the previous study of HCO^+ broadened by Ar,[13] therefore a mechanical pump was used to set a slower flow of gas which allowed the establishment of the discharge at a constant current for the different total gas pressures. For each transition studied, several series of measurements at increasing He pressure were carried out, while maintaining a constant flow of CO/H_2 mixture (in the range 10–15 mTorr) at a constant discharge current (3–9 mA). The maximum pressure of the broadening gas was imposed by the worsening of the signal-to-noise ratio on increasing the total pressure in the cell; this maximum value resulted to be higher than the value of 35 mTorr of ref. [13], thus allowing an investigation over a larger pressure range (see Figures 1 and 2). Another advantage of the slow flow system is the small pressure gradient throughout the cell. By measuring the pressure at both ends of the cell with two pressure gauges (MKS Baratron with a resolution of 0.1 mTorr), one located downstream close to the pumping port (P_{tail}) and the other one close to the gas inlet (P_{head}), it has been verified that $P_{head}-P_{tail}\approx0.2$–$0.8$ mTorr in the range from lower to higher pressure measurements; therefore, in the data analysis the value of the pressure has been assumed to be $P=(P_{head}+P_{tail})/2$.

The Pyrex cell was cooled at 88 ± 2 K by liquid nitrogen circulation in an external plastic pipe wound tightly around it,

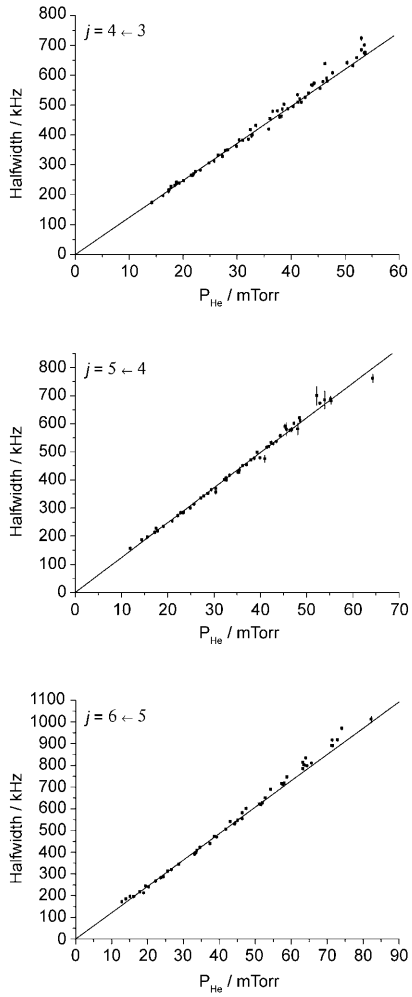

Figure 1. Plots of line widths vs pressure for HCO^+ lines perturbed by He. Top: $j=4\leftarrow3$, middle: $j=5\leftarrow4$, bottom: $j=6\leftarrow5$.

and an axial magnetic field up to about 110 G was applied throughout the length of the discharge. With this longitudinal magnetic field applied, ions are produced and observed in the negative glow,[17] which is a nearly field-free region where they are expected to show no Doppler shift due to the drift velocity, which instead occurs in the positive column[18] where a low axial electric field is present. This absence of Doppler shift has recently been confirmed by Hirao et al.,[19] who compared measurements of DCO^+ transition frequencies previously carried out in this laboratory[20] with new ones obtained with a different experimental apparatus.

A typical spectrum was recorded by sweeping the frequency up and down (several times if signal averaging is needed) in steps of 10 or 15 kHz with an acquisition time of 3 ms per step; the lock-in amplifier time constant was set at 3 ms. For each line 7 to 10 series of measurements at 6 to 9 increasing values of He pressure were carried out, thus obtaining more than 50 data points (line width or shift) to analyze for each transition.

Since the absorption was lower than 6% in any case, collisional line widths Γ and shifts s were recovered from a line

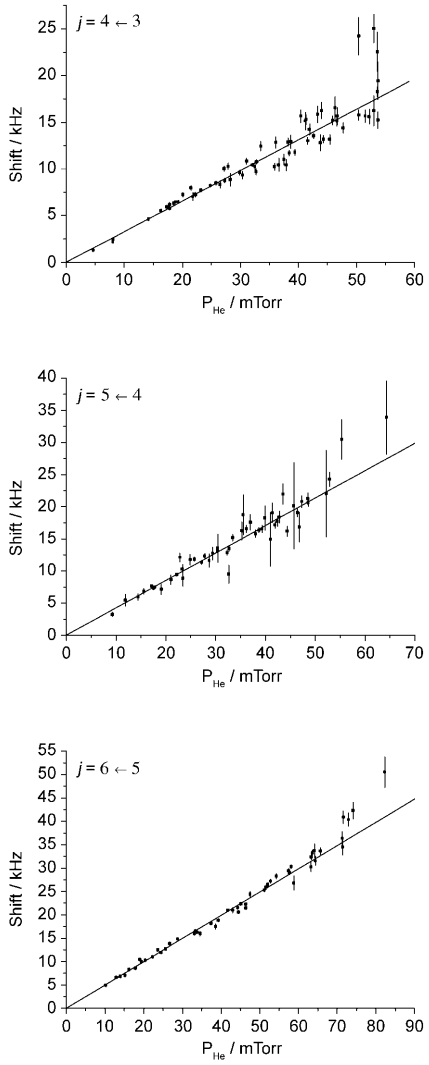

Figure 2. Plots of frequency shifts vs pressure for HCO^+ lines perturbed by He. Top: $j=4\leftarrow3$, middle: $j=5\leftarrow4$, bottom: $j=6\leftarrow5$.

shape analysis of the spectral profile, a procedure which accounts for the frequency modulation and the line asymmetry due to etalon effects in the cell.[16,21] As in ref. [13], the speed-dependent Voigt profile has been used as line shape model,[22] with the Doppler halfwidth $\Delta\nu_D$ set at its value at 88 K ($\Delta\nu_D$/MHz $=3.581\times10^{-7}\nu$/MHz$\sqrt{\frac{T/K}{M/amu}}$). The straight lines in Figure 1 and 2 are obtained from least-squares fitting and their slopes yield the pressure-broadening and the pressure-shift parameters, respectively.

2.2. Construction and Testing of the Potential Energy Surface

For the calculations a conventional Jacobi coordinate system (R,θ) is used where R is the distance of the He atom from the center of mass of HCO^+ and θ is the angle between the CH and the R distance vectors (see Figure 3). For scanning the potential energy surface (PES), the HCO^+ monomer is frozen at

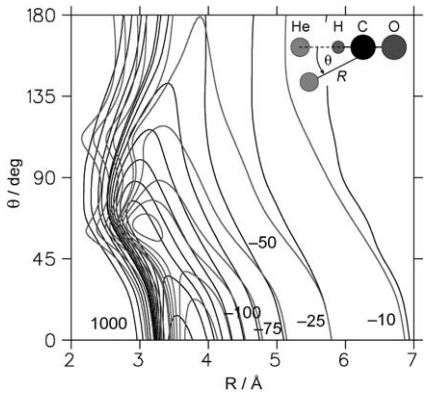

Figure 3. The potential energy surfaces for the He–HCO^+ complex used herein: CCSD(T)/aug-cc-pVQZ (——, current work) and the HF/6-311G PES (——, ref. [9]). The coordinates are the van der Waals distance R and the angle θ. Some contours are labelled with energies in cm^{-1}. The innermost contour for the CCSD(T)/aug-cc-pVQZ PES is at -250 cm^{-1} and at -150 cm^{-1} for the HF/6-311G PES.

its minimum energy structure calculated for the He–HCO^+ complex at the CCSD(T)/aug-cc-pVQZ level using MOLPRO.[23] The bond lengths are $r_{CO}=1.109$ Å and $r_{CH}=1.096$ Å respectively. This compares well with previous calculations at the MP2/aug-cc-pVTZ level ($r_{CO}=1.119$ Å and $r_{CH}=1.092$ Å) and present MP2/aug-cc-pVQZ calculations ($r_{CO}=1.116$ Å and $r_{CH}=1.092$ Å).[24]

It is advantageous to choose the grid on which energies are calculated such as to minimize the effort in the bound state and scattering calculations. Evaluation of the necessary angular integrals is stablest if Gauss–Legendre points are used.[25] In addition, the representation of the interaction potential is simplified. Thus calculations at angles corresponding to an 11-point quadrature ($\theta=11.98^o$, 27.49^o, 43.10^o, 58.73^o, 74.36^o, 90.00^o, 105.64^o, 121.27^o, 136.90^o, 152.51^o and 168.02^o) were performed. In addition, calculations in the two collinear geometries were carried out to assess the accuracy of the fit. The radial R grid included 21 regularly spaced points ($\Delta R=0.1$ Å) between 2.0 Å and 4.0 Å, and additional points at $R=4.25$, 4.50, 4.75, 5.00, 5.50, 6.00, 7.00, 8.00, and 10.00 Å, respectively, which yields 390 points. The total potential $V(R,\theta)$ is represented as Equation (1):

$$V(R,\theta)=\sum_\lambda V_\lambda(R)P_\lambda(\cos\theta) \quad (1)$$

where $V_\lambda(R)$ are the radial strength functions and the sum runs over $\lambda=0$ to 10. It is advantageous to represent the radial strength functions as reproducing kernels,[26] as this allows an exact fit of the ab initio points. According to the radial R^{-4} dependence of the intermolecular potential a kernel given by Equation (2):

$$q_1^{2,4}(x,x')=\frac{2}{15}x_>^{-5}\left(-\frac{5x_<}{7x_>}\right) \quad (2)$$

is used, where $x_>$ and $x_<$ are, respectively, the larger and smaller of x and x'.[26] This kernel explicitly captures the dominant

ion–induced-dipole interaction at long range. Alternative forms exist for weaker dispersion-dominated interactions. Because it is unclear how the high-lying regions of the intermolecular PES depend upon the vibrational state of the HCO^+ monomer, the PES was not adiabatically corrected as was previously done for related systems.[24,27–31]

To test the new PES, the frequencies for the lower bound states and related spectroscopic observables were calculated. Bound state calculations were carried out with the BOUND computer program.[32] The reduced mass of the complex was 3.5171996 amu and the rotational constant of the monomer was fixed at $B=1.48751\ cm^{-1}$.[18] The HCO^+ basis set included internal angular momenta up to $j=30$. This proved to be sufficient for convergence to better than $10^{-4}\ cm^{-1}$. Experimentally, the rotational constants of the ground vibrational state were determined as $B_{0000}=0.2900\ cm^{-1}$ and $D_{0000}=1.00\times10^{-5}\ cm^{-1}$, where (0000) labels the quantum state of the He–HCO^+ complex ($v_{CH}bKn$).[33] The quantum numbers correspond to a bending quantum number b that correlates in the isotropic limit with the HCO^+ rotational quantum number j, the van der Waals stretching quantum number n, the total angular momentum J and its projection K onto the molecule's fixed axis. Using the CCSD(T)/aug-cc-pVQZ PES from the present calculations, $B_{0000}=0.3010\ cm^{-1}$ and $D_{0000}=1.16\times10^{-5}\ cm^{-1}$, which compares favourably with experiment and previous calculations ($B_{0000}=0.2853\ cm^{-1}$ and $D_{0000}=0.94\times10^{-5}\ cm^{-1}$) using an adiabatically corrected PES.[24] The ground state is at $-171.98\ cm^{-1}$ which is $105.30\ cm^{-1}$ above the global minimum. Fundamental bending and stretching modes of He have frequencies of $32.3\ cm^{-1}$ and $42.0\ cm^{-1}$, compared with $36.5\ cm^{-1}$ and $46.4\ cm^{-1}$ from previous work, respectively. Thus, the CCSD(T)/aug-cc-pVQZ PES used here provides a sound basis for further studies in view of the (limited) experimental data and previous calculations on adiabatically corrected QCISD(T) surfaces.

In ref. [9] a different PES was obtained at the SCF/6-311G level from points calculated on a grid of twelve intermolecular distances ranging from 1.9 to 8 Å and of seven angles. A comparison between that potential and the present one is shown in Figure 3. The CCSD(T)/aug-cc-pVQZ PES has a smaller repulsive core and a deeper well while the two potentials are more similar at long distances.

2.3. Scattering Calculations

Calculations are performed for the six lowest rotational lines of the ion by resorting to the impact approximation[34,35] which assumes a relaxation induced by uncorrelated binary collisions. Such a model is reliable in our case because the experimental conditions involve pressures sufficiently low to make the duration of a single collision τ negligible with respect to the average time between two collisions. Moreover, in the experimental spectra the photon frequency ν is generally close to the line peak frequency ν_0 shown in Equation (3):

$$|\nu-\nu_0| \ll 1/2\pi\tau \tag{3}$$

Within this framework the absorption α is described by a Lorentzian shape, Equation (4), with width Γ and shift s

$$\alpha(\nu) \propto \frac{\Gamma}{(\nu-\nu_0-s)^2+\Gamma^2} \tag{4}$$

Since broadening due to causes other than collisions are present, such as Doppler broadening, the Lorentzian in the measurements must be disentangled from other effects, as described in Section 2.1. By this procedure values of Γ and s are obtained that are linear with the pressure p, as shown in Figures 1 and 2. The slope of Γ/p defines the pressure broadening observable, while s/p is the pressure shift. Such a linear dependence also is forecast by the impact theory. The effect of a single collision on a spectral line $i \leftarrow f$ is defined by a complex cross section σ while Γ and s are obtained by multiplying σ by the number of collisions [Eq (5)]:

$$\Gamma - is = n\bar{v}\sigma \tag{5}$$

where $\bar{v}$ is the mean relative velocity and n the perturber density. The contribution to σ of a collision characterized by an ingoing translational state k is described by a complex efficiency function P, which can be obtained from the scattering matrix S given by Equation (6):

$$P(k) = 1 - \sum_{k'} \langle i,k|S|i,k'\rangle\langle f,k'|S^{tr}|f,k\rangle \tag{6}$$

where k' characterizes the outgoing translation state and S^{tr} is the conjugate transpose of the scattering matrix S. In practice, Γ and s are calculated from the scattering matrix S, which also describes the rate constants for state-to-state rotational transitions. Therefore, our experimental check of line shape calculations allows testing a theoretical model that also accounts for the rate constants of astrophysical interest.

In calculating the scattering matrix the ion is treated as a rigid rotor in its ground vibrational state. Indeed, $803.7\ cm^{-1}$ are needed[36] for the transition to the lowest excited state, (0100) in the bound state notation, an energy which is not available in the situation we study. The rotational energies of the ion are obtained using $B=1.4875081333\ cm^{-1}$, $D=2.760799\times10^{-6}\ cm^{-1}$, $H=9.94\times10^{-12}\ cm^{-1}$.[37] It is worthwhile noting that the energies from ref. [18] and used in the PES calculations are slightly different, however such a high degree of accuracy of the rotational energies is not needed for PES or for the scattering calculations. The most accurate available constants are needed for line frequency, however; recently a new set of constants[38] was obtained allowing an accuracy of 10^{-9} for the frequencies.

Semiclassical calculations are performed according to the theoretical model described in detail in ref. [8] which allows the use of our PES. This differs from the more common treatments which restrict themselves to potentials that vary with distance as r^{-n}. It resorts to quantum mechanics for the internal motions of the two colliding partners while it treats classically the orbital motion which is calculated by using the spherical part of the potential. Moreover, for weak collisions that

occur at large impact parameters, the model assumes that the interaction is small and uses a second order perturbative expansion in the potential energy function.

Quantum calculations are carried out with the MOLSCAT computer code.[39] Solving the time-independent Schrödinger equation involves expanding the total wavefunction in the internal basis sets of the colliding species and a partial wave expansion for the angular part of the collision coordinate. Coupled second-order differential equations are obtained for radial functions which are labelled by the quantum numbers of the asymptotic basis and the partial waves. The coupling, which vanishes asymptotically, is due to the intermolecular potential. Truncation of the infinite asymptotic basis sets leads to the close-coupling method. The scattering matrix is obtained by matching the resulting radial functions at large distances to those which would have been obtained in the absence of an interaction potential. A convergence test led us to include in the calculation states of the colliding pair with a maximum total angular momentum J_{max} depending on translation energy and going from 60, at low energy, up to 120, at 300 cm^{-1}. Further tests showed that for converging the scattering matrix it is necessary to include rotational energy levels of HCO^+ up to $j_{max}=21$.

3. Results and Discussion

The results of measurements and calculations are summarized in Table 1. Measurements were carried out for three lines and 99% confidence statistical errors are reported in parentheses. Theoretical results are reported for six lines for which quantum and semiclassical calculations were carried out. For quantum calculations the discrepancy with pressure broadening measurements is in the range of 1–5% whereas shift measurements are larger by about 0.1 MHz $Torr^{-1}$ than theoretical values. This corresponds to a difference of $\approx$30%. The overall agreement can be considered as satisfactory even if in some cases the discrepancy is larger than the statistical error. It is well-known, however, that systematic errors occur in addition to statistical errors in pressure-broadening experiments.[40] They are estimated to be of the order of 2%, in the case of stable species measured in static conditions, and, therefore, they are expected to be larger in the present experiment carried out on flowing gases and with a species generated in a discharge cell. Moreover, the quite large relative error for the shifts is related to a very small shift/width ratio, which makes both measurements and calculations difficult. Indeed, if we consider that broadening and shift are the real and imaginary parts of a complex quantity, the accuracy of the shift is better described by $\Delta s/\Gamma$ than by $\Delta s/s$. If this point of view is adopted, a discrepancy for the shifts of less than 1% of the broadening value is found. Table 1 also shows that a worse agreement is found when semiclassical calculations are used as they overestimate pressure broadening by about 10–15% while they underestimate pressure shift by an order of magnitude. On the whole, comparison between theory and experiment allows discrimination between quantum and semiclassical treatments. As expected, the former proves to be more accurate than the latter.

Table 1. Measured and calculated broadening and shift parameters of HCO^+ rotational lines perturbed by helium at 88 K. Units are MHz/Torr for broadening and shift while line frequencies are in MHz.

Line	Frequency[38]	Parameter	Exp.[a]	Quantum	Semiclassical
1←0	89 188.5261	Broadening	–	13.76	15.49
		Shift	–	0.154	0.07
2←1	178 375.0642	Broadening	–	13.01	15.17
		Shift	–	0.168	0.09
3←2	267 557.6263	Broadening	–	12.64	14.81
		Shift	–	0.134	0.07
4←3	356 734.2246	Broadening	12.39(29)	12.27	14.42
		Shift	0.328(19)	0.229	0.05
5←4	445 902.8713	Broadening	12.42(22)	11.95	14.06
		Shift	0.427(29)	0.312	0.04
6←5	535 061.5791	Broadening	12.13(29)	11.72	13.73
		Shift	0.497(17)	0.364	0.03

[a] 99% confidence intervals are reported in parentheses.

All the theoretical data in Table 1 were calculated by integrating over the thermal energy distribution given by Equation (7):

$$\sigma = \frac{1}{(kT)^2}\int_0^\infty E e^{-E/kT}\sigma(E)dE \qquad (7)$$

and not at the mean relative translational energy $\bar{E}=4kT/\pi$ (77.87 cm^{-1} at 88 K). Indeed, as shown in Table 2, mean energy calculations involve non-negligible errors, particularly when the shift is considered. In order to reduce computing time, this kind of error is frequently neglected and one resorts to mean energy calculation. Such an approximation is likely not to be very accurate, even within the semiclassical model and is still worse when a full quantum treatment is used. A major reason for this is the occurrence of quantum resonances, such as those shown in Figure 4 for the $j=1\leftarrow0$ and $j=6\leftarrow5$ transitions. Indeed, the energy dependence of shift and width exhibits quite irregular oscillations for all lines studied. Such oscillations make mean energy calculations unreliable because $\bar{E}$ may fall on a maximum or a minimum of the oscillation. Moreover, the integration over E is numerically unstable because of the high-frequency oscillations, and the 6-point Gaussian quadrature implemented in MOLSCAT is not suitable. We resorted to an adaptive integration with a large number of energy points to achieve convergence. This number changes from line to line

Table 2. Comparison between cross sections obtained at mean energy and those obtained by integration over the thermal energy distribution. Units are [$Å^2$].

Line	By integration		At mean energy	
	Re σ	Im σ	Re σ	Im σ
1←0	110.05	1.23	111.63	3.78
2←1	104.06	1.33	107.74	1.08
3←2	101.04	1.12	103.07	0.54
4←3	98.19	1.83	99.51	1.48
5←4	95.66	2.51	94.46	1.95
6←5	93.79	2.89	91.51	2.52

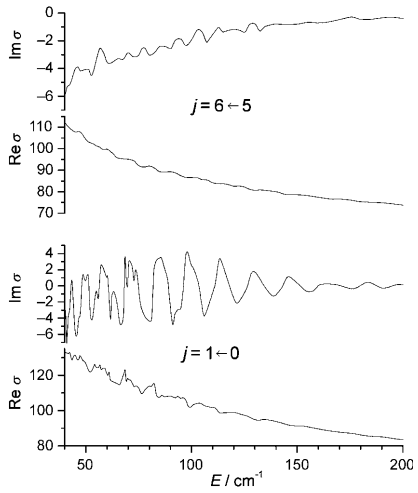

Figure 4. Dependence of σ on orbital energy E for $j=6\leftarrow5$ and $j=1\leftarrow0$. Units are Å^2.

and ranges between 112 (for lines with high j values) to 198 (for lines with small j values).

Oscillations similar to those displayed in Figure 4 were found in low-energy calculations of CO perturbed by Helium.[41] There it was suggested that such quantum resonances should be more pronounced when less energy is needed to excite the collisional transition. This is in agreement with our evidence of a larger effect for lines at lower j values, as can be seen from Figure 4 by comparing the cases $j=1\leftarrow0$ and $j=6\leftarrow5$. It is worthwhile noting that oscillations tend to damp down when E increases and to disappear when E is comparable to the well depth of the potential well, which for our potential is $D_e=-172$ cm^{-1} and $D_0=-277$ cm^{-1}.

Table 3 compares the theoretical results obtained by using our new potential to those obtained by the potential of ref. [9]. The difference is small; for the three lines measured it is less than 3% for the broadening and less than 10 kHz Torr^{-1} for the shift. Thus, comparison with the experimental data does not allow favouring one PES over the other one. It is somewhat surprising that two such different PESs (see Figure 3) give almost equal line shape parameters. In order to understand this result better, the new PES was modified by a controllable coordinate transformation, as proposed in ref. [14]. By an arbitrary function f, r is scaled to r' [Eq. (8)]:

Table 3. Comparison between the line shape parameter calculated by the present potential and those calculated by the potential of ref. [9]. Units are [MHz Torr^{-1}].

Line	Potentials herein		Potential of ref. [9]	
	Broadening	Shift	Broadening	Shift
1←0	13.76	0.154	14.08	0.201
2←1	13.01	0.168	13.46	0.124
3←2	12.64	0.134	12.97	0.163
4←3	12.27	0.229	12.57	0.225
5←4	11.95	0.312	12.07	0.304
6←5	11.72	0.364	11.52	0.373

$$r' = f(r) \tag{8}$$

and the true potential $V(r,\theta)$ is changed ("morphed") to Equation (9):

$$V'(r,\theta) = V(r',\theta) = V[f(r),\theta]. \tag{9}$$

We use two different functions f, one (f_{short}) given by Equation (10) affecting mainly the short-range repulsive part of the potential, and the other (f_{long}) given by Equation (11) mainly modifying the long-range attractive part:

$$f_{\text{short}}(r) = r\left[1 - \frac{p}{2}\left(1 - \tanh\frac{r-r_0}{d}\right)\right] \tag{10}$$

or

$$f_{\text{long}}(r) = r\left[1 - \frac{p}{2}\left(1 + \tanh\frac{r-r_0}{d}\right)\right] \tag{11}$$

The parameter p controls the magnitude of scaling; indeed, f_{short} in Equation (10) yields $r' \simeq r(1-p)$ for small r values and $r' \simeq r$ for large r values, while the opposite is true for f_{long} in Equation (11). In Equation (10) we used $r_0=2.5$ Å and $d=0.5$ Å, while we used $r_0=3.7$ Å and $d=0.8$ Å in Equation (11). We consider scaling from 20% down to 20% up, that is to say, we use the values $p=-0.2$, -0.1, 0.1, 0.2 and $p=0$ corresponding to the true potential. Figure 5 shows the effect of such a scaling on the isotropic part, V_0, of the PES. For all other Legendre components the effect is similar.

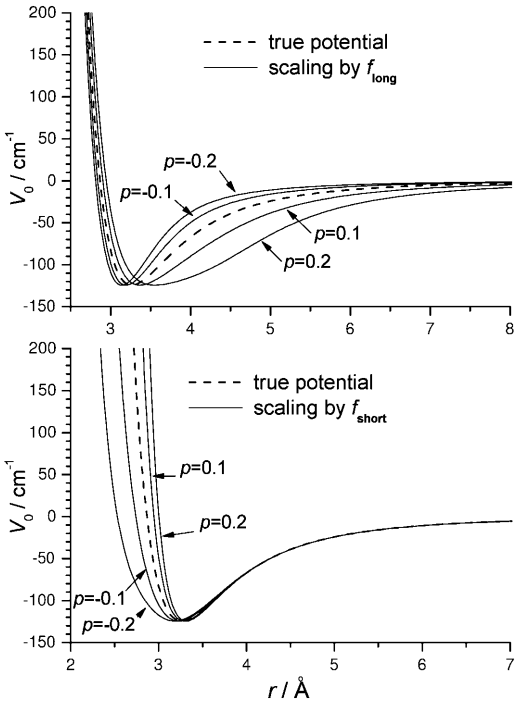

Figure 5. Effect on the spherical part of the potential of a distance scaling acting mainly either at short or at long distances. See Equations (8)–(11). Four values of the scaling parameter p are used. $p=0$ corresponds to the true potential.

Quantum scattering calculations are performed for the rotational transition $j=4\leftarrow3$. The results obtained for different values of p are summarized in Table 4 and Figure 6. Γ is considerably more sensitive to the long- than to the short-range part of the potential. From a phenomenological perspective, the broadening cross section (Re σ) essentially scales with the square of the radius of the attractive part. For example, for f_{long} with $p=-0.1$, the diameter of the long-range attractive part of the potential decreases by 10% and the cross section is smaller by about 20% compared to what is obtained from the unmorphed potential ($p=0$). From Figure 6b one can see that a few% change in the long-range part of the potential would cause the calculated value of Re σ (▲) to be in disagreement with measurement. By using f_{short} to morph the PES, the effect on pressure broadening is smaller by one order of magnitude compared to scaling of the long-range part, thus, a 10% change in the radius affects the cross section by only about 2%. Comparison between calculations (●) and measurements does not allow the exclusion of a repulsive core different by 10–20% from the one we used.

Table 4. Effect on the calculated cross section of a PES modified by a distance scaling acting mainly either at short distances (f_{short}) or at long distances (f_{long}) for line $j=4\leftarrow3$. See Equations (10) and (11) and Figure 5. Parameter p sets the magnitude of the scaling and $p=0$ means no scaling.

p	f_{short} Re σ	Im σ	f_{long} Re σ	Im σ
0.2	93.74	2.25	165.91	0.48
0.1	95.29	2.02	126.95	1.50
0.0	98.19	1.83	98.19	1.83
0.1	100.81	1.34	78.61	1.53
0.2	102.54	1.22	67.15	1.36

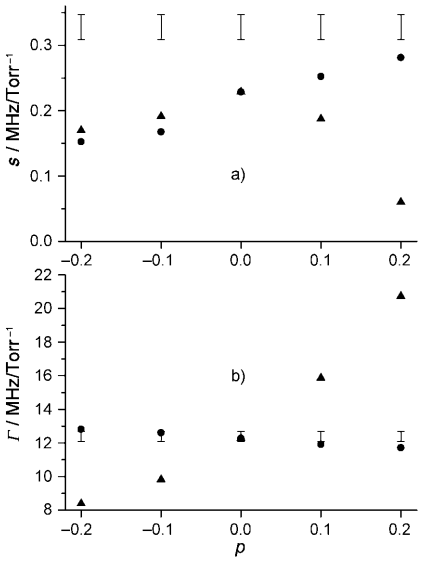

Figure 6. Effect of potential changes on a) pressure broadening and b) shift of the line $j=4\leftarrow3$. Measurements (error bars) are compared to calculations done by a potential scaled either at short distances [●, see Eq. (10)] or at long distances [▲, see Eq. (11)]. The parameter p sets the magnitude of potential changes [See Eqs. (10) and (11)].

The trend of the shift cross sections Im σ is less clear. Indeed, a simple interpretation of the shift effect is particularly difficult when it is a small fraction of the broadening, as is the case for $He–HCO^+$. While broadening is essentially a sum of the effect of collisions on the two states involved in the transition, the shift is mostly a difference between two effects, which, when the shift/width ratio is small, are almost equal. In a sense, pressure shift is a higher-order effect. Thus, based on the present results, the sensitivity of the pressure shift on particular regions of the PES is not further analyzed. Additional experimental information from systems with a higher shift/width ratio, such as HF–Ar, are required for this.[42]

These considerations also allow us to return to the question which drew our attention to the problem, namely the small difference between calculations on the CCSD(T)/aug-cc-pVQZ level and the PES of ref. [9]. Most likely this observation is related to the similar long-range parts of the two PESs which are dominated by charge–induced-dipole and dipole–induced-dipole interactions. From a more general perspective it is worthwhile to mention that spectroscopic bound state and spectral broadening data are sensitive to different parts of the PES. Thus, the combination of this information will allow a better definition of the overall shape of the interaction potential. Finally, the present results also explain why the first line-broadening calculations[43,44] could obtain quite a good agreement by considering only the long-range electrostatic part of the potential.

Acknowledgements

M.M. acknowledges financial support from the Schweizerischer Nationalfonds (grant 200021-117810) and partial support through the EU network "Molecular Universe". L.D. and F.T. acknowledge financial support from MIUR (PRIN 2005 funds, project "Trasferimenti di energia e di carica a livello molecolare") and University of Bologna (RFO funds).

Keywords: ab initio calculations · collisions · helium · potential energy surfaces · rotational spectroscopy

[1] E. Herbst, W. Klemperer, *Astrophys. J.* **1974**, *188*, 255–256.
[2] B. E. Turner, *Astrophys. J.* **1974**, *193*, L83–L87.
[3] S. Green, *Astrophys. J.* **1975**, *201*, 366–372.
[4] T. G. Anderson, C. S. Gudeman, T. A. Dixon, R. C. Woods, *J. Chem. Phys.* **1980**, *72*, 1332–1336.
[5] R. C. Woods in *Molecular Ions: Spectroscopy, Structure, and Chemistry*, (Eds.: T. A. Miller, V. E. Bondybey), North Holland, Amsterdam, **1983**, and references therein.
[6] E. Herbst, *J. Phys. Conf. Ser.* **2005**, *4*, 17–25.
[7] T. Monteiro, *Mon. Not. R. Astron. Soc.* **1985**, *214*, 419–427.
[8] G. Buffa, *Phys. Rev. A* **2007**, *76*, 042509.
[9] T. Monteiro, *Mon. Not. R. Astron. Soc.* **1984**, *210*, 1–11.
[10] G. Buffa, O. Tarrini, G. Cazzoli, L. Dore, *Phys. Rev. A* **1994**, *49*, 3557–3565.
[11] Q. Liao, E. Herbst, *J. Chem. Phys.* **1996**, *104*, 3956–3961.
[12] G. Buffa, O. Tarrini, G. Cazzoli, L. Dore, *J. Chem. Phys.* **1999**, *111*, 1870–1874.

[13] G. Buffa, L. Dore, F. Tinti, M. Meuwly, *ChemPhysChem* **2006**, *7*, 1764–1769.
[14] M. Meuwly, J. M. Hutson, *J. Chem. Phys.* **1999**, *110*, 8338–8347.
[15] B. Gazdy, J. M. Bowman, *J. Chem. Phys.* **1991**, *95*, 6309–6316.
[16] G. Cazzoli, L. Dore, *J. Mol. Spectrosc.* **1990**, *141*, 49–58.
[17] F. C. De Lucia, E. Herbst, G. M. Plummer, G. A. Blake, *J. Chem. Phys.* **1983**, *78*, 2312–2316.
[18] K. V. L. N. Sastry, E. Herbst, F. C. De Lucia, *J. Chem. Phys.* **1981**, *75*, 4169–4170.
[19] T. Hirao, S. Yu, T. Amano, *J. Chem. Phys.* **2007**, *127*, 074301.
[20] P. Caselli, L. Dore, *Astron. and Astrophys.* **2005**, *433*, 1145–1152.
[21] L. Dore, *J. Mol. Spectrosc.* **2003**, *221*, 93–98.
[22] J. F. D'Eu, B. Lemoine, F. Rohart, *J. Mol. Spectrosc.* **2002**, *212*, 96–110.
[23] MOLPRO is a package of ab initio programs written by H. J. Werner, with contributions from R. D. Amos, P. J. Knowles, A. Bernhardsson, A. Berning, P. Celani, D. L. Cooper, M. J. O. Deegan, A. J. Dobbyn, F. Eckert, C. Hampel, G. Hetzer, T. Korona, R. Lindh, A. W. Lloyd, S. J. McNicholas, F. R. Manby, W. Meyer, M. E. Mura, A. Nickiass, P. Palmieri, R. Pitzer, G. Rauhut, M. Schütz, H. Stoll, A. J. Stone, R. Tarroni, T. Thorsteinsson, H. J. Werner and P. J. Knowles. MOLPRO, Version 2000, University of Birmingham, Birmingham, **2000**.
[24] M. Meuwly, *J. Chem. Phys.* **1999**, *111*, 2633–2640.
[25] M. Meuwly, J. M. Hutson, *J. Chem. Phys.* **1999**, *110*, 3418–3427.
[26] T. S. Ho, H. Rabitz, *J. Chem. Phys.* **1996**, *104*, 2584–2597.
[27] M. Meuwly, R. J. Bemish, *J. Chem. Phys.* **1997**, *106*, 8672–8680.
[28] M. Meuwly, *J. Chem. Phys.* **1999**, *110*, 4347–4353.
[29] A. A. Buchachenko, N. F. Stepanov, R. V. Krems, S. Nordholm, *Phys. Chem. Chem. Phys.* **2002**, *4*, 4992–4998.
[30] M. Meuwly, P. P. Wolynec, E. J. Bieske, *J. Chem. Phys.* **2002**, *116*, 4948–4954.
[31] S. P. Belov, B. A. McElmurry, R. R. Lucchese, J. W. Bevan, I. Leonov, *Chem. Phys. Lett.* **2003**, *370*, 528–534.
[32] J. M. Hutson, Bound computer program, version 5. Distributed by the Collaborative Computational Project No. 6 of the UK Engineering and Physical Sciences Research Council, **1993**.
[33] S. A. Nizkorodov, J. P. Maier, E. J. Bieske, *J. Chem. Phys.* **1995**, *103*, 1297–1302.
[34] M. Baranger, *Phys. Rev.* **1958**, *112*, 855–865.
[35] U. Fano, *Phys. Rev.* **1963**, *131*, 259–268.
[36] C. Puzzarini, R. Tarroni, P. Palmieri, S. Carter, L. Dore, *Mol. Phys.* **1996**, *87*, 879–898.
[37] G. A. Blake, K. B. Laughlin, R. C. Cohen, K. L. Busarow, R. J. Saykally, *Astrophys. J.* **1987**, *316*, L45–L48.
[38] F. Tinti, L. Bizzocchi, C. Degli Esposti, L. Dore, *Astrophys. J.* **2007**, *669*, L113–L116.
[39] J. M. Hutson, S. Green, MOLSCAT computer code, version 14 (1994), distributed by Collaborative Computational Project No. 6 of the Science and Engineering Research Council (UK).
[40] J.-M. Colmont, B. Bakri, F. Rohart, G. Wlodarczak, J. Demaison, G. Cazzoli, L. Dore, C. Puzzarini, *J. Mol. Spectrosc.* **2005**, *231*, 171–187.
[41] C. D. Ball, F. C. De Lucia, *Phys. Rev. Lett.* **1998**, *81*, 305–308.
[42] J.-M. Hartmann, C. Boulet, *J. Chem. Phys.* **2000**, *113*, 9000–9010.
[43] P. W. Anderson, *Phys. Rev.* **1949**, *76*, 647–661.
[44] C. T. Tsao, I. Curnutte, *J. Quant. Spectrosc. Radiat. Transfer* **1962**, *2*, 41–91.

Received: June 17, 2008
Published online on September 22, 2008

